Exploring the structural dynamics of the translational machinery using single-molecule fluorescence resonance energy transfer

22

Daniel D. MacDougall and Ruben L. Gonzalez, Jr.

1. Introduction

The ribosome can be regarded as a molecular machine that converts chemical and thermal energy into productive mechanical work (Spirin, 2002; Frank and Gonzalez, 2010). This chemo- and thermomechanical view of ribosome function is fueling current efforts to identify the mobile components of the ribosomal machine, characterize the structural dynamics of these components, and develop an understanding of how these dynamics are regulated in order to direct mechanical processes during protein synthesis. It is within this context that single-molecule fluorescence resonance energy transfer (smFRET) (Ha, 2001) has emerged as a powerful tool for investigating the structural dynamics and mechanical properties of the translating ribosome. Because this chapter marks its first appearance in this volume, the first half of this chapter provides a brief introduction to smFRET that is specifically framed around its use as a tool for investigating the structural dynamics of the translational machinery. Our intent here is not to provide a comprehensive or detailed review of smFRET (for that we refer the reader to excellent reviews by Ha and co-workers (Ha, 2001; Roy et al., 2008)), but rather to provide a basic understanding of the technique and highlight the strengths and limitations that are most important for understanding and interpreting smFRET studies of protein synthesis.

In the second half of this chapter, we use one of the most dynamic steps in protein synthesis, the movement of the messenger RNA (mRNA)-transfer RNA (tRNA) complex through the ribosome during the translocation step of translation elongation, as an example with which to demonstrate the unique mechanistic information that can be obtained from smFRET studies of protein synthesis. Specifically, we describe how smFRET studies of ribosomal pre-translocation complexes have enabled the discovery and characterization of thermally activated structural fluctuations of the pre-translocation complex. We discuss in detail how modulations of these fluctuations are used to regulate and drive the translocation reaction. We close by briefly highlighting how similar results from smFRET studies of additional steps in protein synthesis are giving rise to new paradigms describing the mechanism and regulation of protein synthesis.

2. Single-molecule fluorescence resonance energy transfer

2.1. Physical principles underlying fluorescence resonance energy transfer

Fluorescence resonance energy transfer (FRET) (Förster, 1946) is a photophysical process involving two fluorophores, termed the donor and the acceptor. In a typical FRET experiment, the donor is directly illuminated by an excitation light source and, upon absorption of a photon, undergoes a transition to an excited electronic state. From its excited state, the donor can emit a photon and relax back to its ground electronic state, a process known as fluorescence. Alternatively, the excited donor can transfer energy to the acceptor *via* a non-radiative dipole-dipole coupling mechanism known as FRET, such that the acceptor now undergoes a transition to an excited electronic state. Subsequent relaxation of the acceptor back to its electronic ground state through the emission of a photon now results in fluorescence from the acceptor.

The efficiency of FRET (E_{FRET}) is given by $E_{FRET} = (1 + (R/R_0)^6)^{-1}$ where R is the distance between the donor and acceptor dipoles and R_0, known as the Förster

distance, is the value of R at which $E_{FRET} = 0.50$ (Figure 1A). R_0 for a specific donor-acceptor pair is a constant that is given by $R_0 = 9.78 \times 10^3 (\Phi_D \bullet k^2 \bullet n^{-4} \bullet J(\lambda))^{1/6}$ where Φ_D is the fluorescence quantum yield of the donor in the absence of the acceptor, k^2 is a geometric factor that depends on the relative orientation of the donor and acceptor transition dipole moments, n is the refractive index of the medium in which the energy transfer occurs, and $J(\lambda)$ is the overlap between the fluorescence emission spectrum of the donor and the absorbance spectrum of the acceptor. Thus, while E_{FRET} scales with the inverse sixth power of R, precise determination of an absolute distance using an experimentally measured value of E_{FRET} requires either careful determination of R_0 (including Φ_D, k^2, n, and $J(\lambda)$) or, more practically, careful experimental calibration of E_{FRET} *versus* R using a biomolecule of known conformation and thus known R. Depending on the specific donor-acceptor pair used, typical values of R_0 render E_{FRET} sensitive to distances in the range of 10–100 Å. This exquisite sensitivity to distances on the Å length scale makes E_{FRET} an effective molecular ruler that has evolved into a powerful biophysical tool for investigating biomolecular structure and dynamics.

2.2. Single-molecule studies uncover unique mechanistic information

Ensemble FRET experiments have been in widespread use for over fifty years and have provided unprecedented insights into the structure and dynamics of biomolecules and biomolecular complexes (reviewed in (Wu and Brand, 1994; Clegg, 1995; Selvin, 1995, 2000; Jares-Erijman and Jovin, 2003; Hwang et al., 2009)). However, because ensemble FRET experiments report the mean value of E_{FRET} averaged over the trillions of individual biomolecules that collectively form the ensemble, any heterogeneity in the structure or dynamics of the biomolecules comprising the ensemble can generate a distorted mean value of E_{FRET} that is difficult or even impossible to interpret. Such heterogeneity can be generally divided into two categories: static heterogeneity, which originates from variations in the structure or dynamics of individual biomolecular subpopulations across the ensemble, and dynamic heterogeneity, which originates from the asynchronous transitioning of individual biomolecules between multiple states, each of which is structurally or dynamically distinct (Hwang et al., 2009). Single-molecule FRET (smFRET) experiments complement ensemble FRET experiments by permitting the ensemble of biomolecules to be dissected into sub-populations (in the case of static heterogeneity) and/or states (in the case of dynamic heterogeneity), each of which exhibit characteristic structural and/or dynamic properties (Figure 1B and C). In so doing, smFRET experiments provide a powerful opportunity to investigate the structural, dynamic, and biochemical properties of individual subpopulations or states.

The ability to parse static and dynamic heterogeneity using smFRET can be of great mechanistic importance; this is because both types of heterogeneity can be exploited to regulate reaction mechanisms. As an example of mechanistically important dynamic heterogeneity, consider an enzyme that exists in a dynamic equilibrium between multiple conformational states, but where, in an extreme case, only one state can progress along the reaction pathway. In such a situation, precise control over the rate with which this state is sampled by the individual enzyme molecules within the ensemble and/or over the stability of this state relative to the other accessible states, provides an effective mechanism for regulating the enzymatic reaction. By permitting the identification and characterization of individual states, including functionally competent states, smFRET experiments provide an opportunity to collect mechanistically important data that are unique from, and complementary to, that obtained from ensemble FRET experiments.

2.3. Design of donor-acceptor labeling schemes

Perhaps the most significant challenges to smFRET studies of the translational machinery are the design of donor-acceptor labeling schemes and the technical challenges involved in the fluorescence labeling of translation components. To be mechanistically informative, donor-acceptor labeling schemes must be designed and implemented such that the structural rearrangement of interest yields a change in the distance between the donor and the acceptor that generates an experimentally detectable change in E_{FRET}. The fluorescence labeling of translation components that is required to meet this criterion must be: (i) efficient, such that a large population of the observed ribosomal complexes contain both a donor and an acceptor; (ii) specific, such that any heterogeneity detected within the ensemble of ribosomal complexes reflects static or dynamic heterogeneity of the complexes rather than heterogeneity in the positions of the donor or accep-

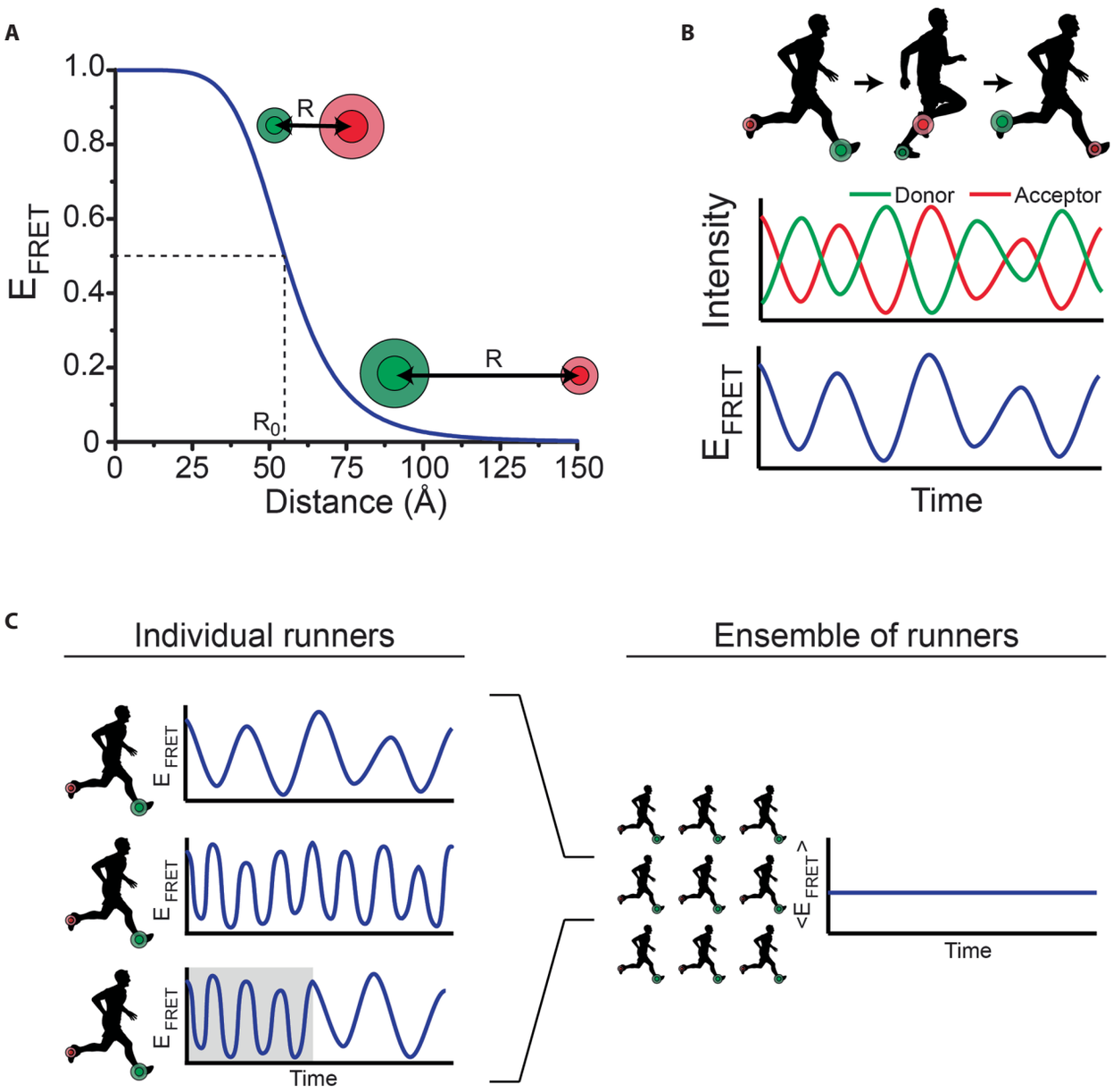

Fig. 1 FRET at the single-molecule and ensemble levels. (A) Plot of the FRET efficiency (E_{FRET}) as a function of the distance (R) between a donor fluorophore (green sphere) and an acceptor fluorophore (red sphere) with an R_0 of 55 Å. When $R < R_0$, $E_{FRET} > 0.50$, when $R = R_0$, $E_{FRET} = 0.50$, and when $R > R_0$, $E_{FRET} < 0.50$. (Adapted from (Roy et al., 2008) with permission from Macmillan Publishers Ltd). (B) A macroscopic example of a FRET experiment. Consider a single runner with a donor-acceptor pair attached to his sneakers (artwork based on an original illustration from iStockPhoto. com, (Laurence Dean). As the runner strides, the distance between the donor-acceptor pair periodically increases and decreases. Consequently, the donor and acceptor emission intensities (I_A and I_D, respectively) *versus* time trajectory yields periodic, anti-correlated increases and decreases in I_A and I_D that are characteristic of FRET. Likewise, the corresponding E_{FRET} *versus* time trajectory (where $E_{FRET} = I_A / (I_A + I_D)$) exhibits periodic increases and decreases in E_{FRET}. From this E_{FRET} *versus* time trajectory it is possible to determine the average stride length and rate of the runner, information that is critical to a full description of the mechanics of running. (C) Representative E_{FRET} *versus* time trajectories from three sub-populations of runners that can be distinguished by their different stride rates (left panel). Static heterogeneity arises from sub-populations of runners with either slow (top row) or fast (middle row) stride rates. Dynamic heterogeneity arises from a sub-population of runners (bottom row) who stochastically alternate between fast (grey shaded box) and slow stride rates. Despite this heterogeneity, analysis of hundreds of individual E_{FRET} *versus* time trajectories can provide the average stride rates of the slow and fast sub-populations of runners (or slow and fast phases of running), information that would be obscured in the ensemble-averaged E_{FRET} ($<E_{FRET}>$) *versus* time trajectory of the ensemble of runners (right panel).

tor; and (iii) minimally perturbative, such that the presence of the donor-acceptor pair does not significantly interfere with the biochemical activities of the relevant translation components. Over the past several years, we and others have developed highly purified *in-vitro* translation systems which, in combination with a battery of previously developed standard biochemical assays, have allowed development and validation of numerous donor-acceptor labeling schemes for smFRET studies of protein synthesis (reviewed in (Frank and Gonzalez, 2010) and discussed below in Section 3.3). Rather than providing a detailed description of the design, implementation, and validation of donor-acceptor labeling schemes here, we instead refer the reader to a recently published chapter on this topic (Fei et al., 2010) and dedicate the remainder of this section to a discussion of the optical setup for smFRET experiments and analysis of the resulting data.

2.4. Total internal reflection fluorescence microscopy

The most important requirement for the detection of fluorescence emission from single molecules is a highly sensitive fluorescence microscope. A total internal reflection fluorescence microscope (TIRFM), which combines a totally internally reflected laser illumination source with wide-field optics and an electron-multiplying charge-coupled device (EMCCD) camera detector, offers such sensitivity (Axelrod et al., 1984; Axelrod, 2003; Joo and Ha, 2007) (Figure 2A). In a typical, prism-based TIRFM, the laser beam is aligned, collimated, and focused through a fused silica prism onto a quartz microfluidic flowcell. Upon encountering the interface between the quartz, having an index of refraction n_q, and the aqueous buffer containing the fluorescence-labeled ribosomal complexes, having an index of refraction $n_b < n_q$, the incident laser beam is totally internally reflected away from the quartz-buffer interface and back into the quartz at all angles greater than the "critical angle," θ_c, given by $\theta_c = \sin^{-1} n_b/n_q$. Regardless of the total internal reflection of the incident laser beam at the quartz-buffer interface, a weak evanescent electromagnetic field propagates into the medium of lesser index of refraction (i. e. the buffer) in the plane of incidence of the laser beam and in a direction that runs parallel along the quartz-buffer interface. The intensity of the weak evanescent field decays exponentially with increasing distance from the quartz-buffer interface, therefore selectively illuminating only a thin layer of the buffer that is adjustable within a depth range of 70–300 nm. Because the excitation of molecules in the bulk buffer is limited by localization of the evanescent field to a thin layer of the buffer just beyond the quartz-buffer interface, the signal-to-noise ratio of a TIRFM is significantly greater than a conventional epi-fluorescence microscope, yielding very high sensitivity fluorescence detection.

Since the evanescent field generated by total internal reflection is confined to a thin layer of buffer just beyond the quartz-buffer interface, it is necessary to localize ribosomal complexes near the quartz surface of the microfluidic flowcell (Figure 2B). As a result, various approaches have been developed for tethering ribosomal complexes to the quartz surface in a manner that brings them within the evanescent field while preserving their biochemical activity (Blanchard et al., 2004b; Uemura et al., 2007; Wang et al., 2007). All such approaches combine a surface passivation method that renders the quartz surface relatively inert to non-specific binding of translation components with an affinity-based surface tethering method that allows specific tethering of ribosomal complexes (Rasnik et al., 2005). The most commonly used method involves passivating the quartz surface with a mixture of polyethylene glycol (PEG) and biotinylated PEG (Ha et al., 2002). Subsequent incubation of the PEG- and biotinylated PEG-derivatized microfluidic flowcell with streptavidin, followed by incubation with a ribosomal complex assembled onto a biotinylated messenger mRNA (mRNA) (Blanchard et al., 2004b) or, alternatively, a directly biotinylated ribosomal subunit (Wang et al., 2007), then allows tethering of the ribosomal complex *via* a biotin-streptavidin-biotin bridge. In addition to confining ribosomal complexes within the evanescent field, surface tethering allows the fluorescence emission from individual, spatially localized donor-acceptor pairs to be observed for extended periods of time, limited only by the irreversible, oxygen-mediated photobleaching of the donor or acceptor (Hubner et al., 2001; Piwonski et al., 2005; Renn et al., 2006). It should be noted that observation times in smFRET experiments are typically extended through the use of enzymatic oxygen scavenging systems (Benesch and Benesch, 1953; Patil and Ballou, 2000; Ha, 2001; Aitken et al., 2008) and the photostabilities of the fluorophores are additionally enhanced through the addition of small-molecule triplet-state quenchers that suppress unwanted blinking of the fluorophores (Gonzalez Jr. et al., 2007; Aitken et al., 2008; Dave et al., 2009).

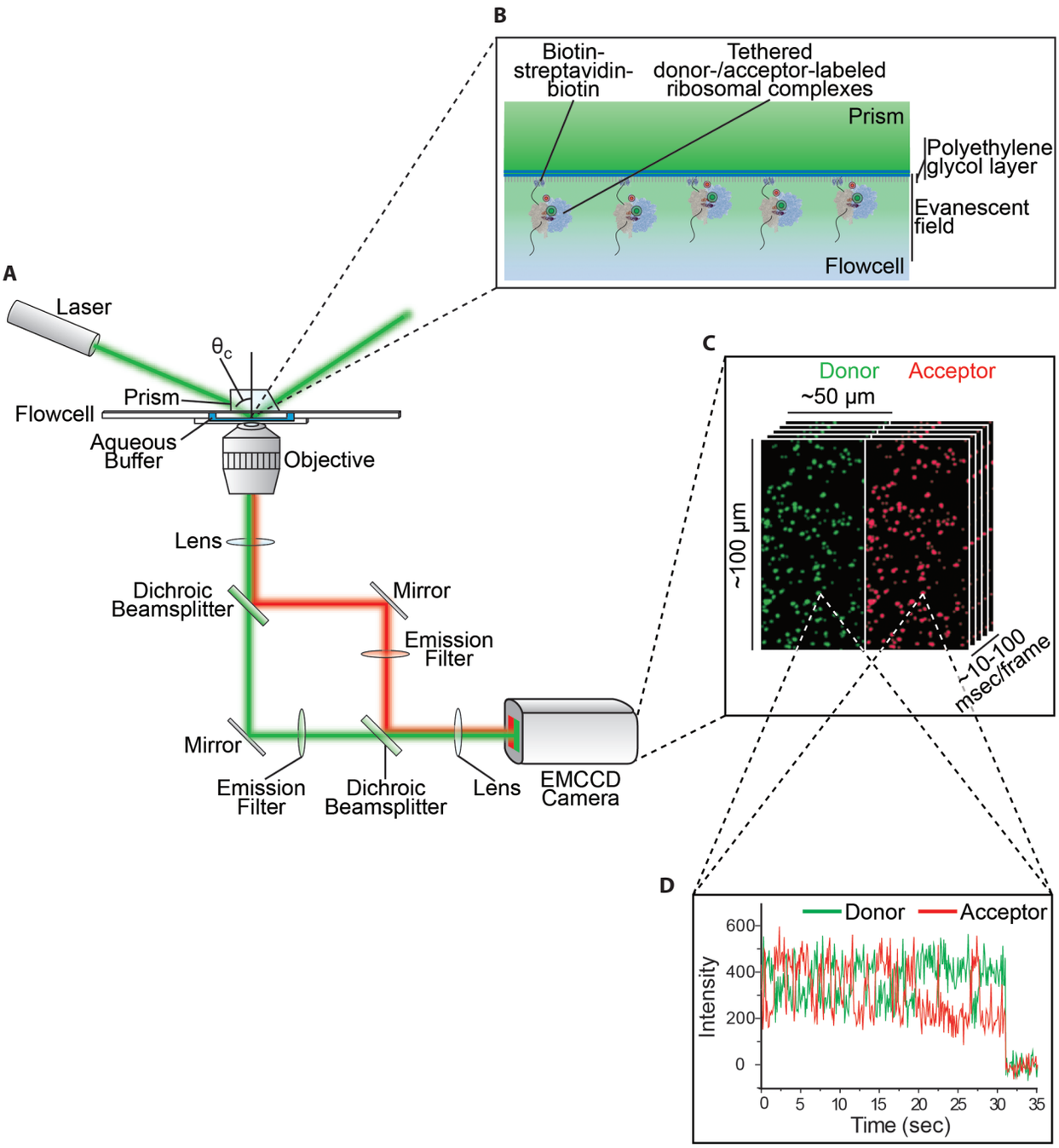

Fig. 2 Single-molecule fluorescence detection using a prism-based total internal reflection fluorescence microscope. (A) Principles of operation and typical optical setup up of a total internal reflection fluorescence microscope. See Section 2.4for a detailed description. (B) Inset showing an enlargement of the quartz/buffer interface and depicting the tethering of donor-/acceptor-labelled ribosomal complexes onto the polyethylene glycol (PEG)/biotinylated PEG-passivated quartz surface using a biotin-streptavidin-biotin bridge. See Section 2.4for a detailed description. (C) Inset showing an enlargement of a single image recorded by the EMCCD. Typically, the donor and acceptor signals from 200–400 spatially resolved ribosomal complexes located within a 100 µm (50 µm field-of-view are simultaneously imaged onto two separate halves of the capacitor array within the EMCCD camera. Individual images are recorded as a digital video with a typical frame rate in the tens of frames per sec (i. e. a time resolution in the tens of msec per frame). (D) Representative donor and acceptor emission intensities *versus* time trajectory derived from a single donor-/acceptor-labeled ribosomal complex within the field-of-view (Fei et al., 2009).

In addition to the high sensitivity arising from its total internal reflection illumination mode, the TIRFM is a wide-field instrument, therefore allowing simultaneous excitation and detection of fluorescence signals from several hundred individual ribosomal complexes. Upon selective donor excitation *via* total internal reflection illumination, fluorescence emissions from several hundred spatially localized donor-acceptor pairs, each arising from a single surface-tethered ribosomal complex, are simultaneously collected through a microscope objective. A system of lenses, dichroic beamsplitters, mirrors, and emission filters is then used to: (i) separate the emitted fluorescence into individual donor and acceptor channels; (ii) filter out any remaining traces of the total internally reflected illumination source from each channel; and (iii) direct the two channels to the EMCCD camera such that the donor and acceptor signals from several hundred spatially resolved ribosomal complexes are simultaneously imaged onto two separate sectors of the capacitor array within the EMCCD camera (Figure 2C). Individual images are recorded as a digital video with a typical frame rate in the tens of frames per sec (i. e. a time resolution in the tens of msec per frame). Despite the limited time resolution, it is the combination of the TIRFM's wide-field operation and high sensitivity that has thus far made it the instrument of choice for smFRET studies of protein synthesis.

2.5. Limitations of single-molecule fluorescence microscopies

Despite the current dominance of TIRFM, it is important to note a few limitations of this approach that significantly impact smFRET studies of protein synthesis. One limitation of TIRFM is the experimental time resolution, which is restricted by the rate with which the EMCCD camera reads out an individual frame. Using the typical settings on a current state-of-the-art EMCCD camera, the time resolution is limited to tens of msec per frame. Even using settings allowing for the maximal readout rate, albeit at the expense of significantly reduced signal-to-noise ratio, the time resolution of a current state-of-the-art EMCCD camera is limited to several msec per frame (Cornish and Ha, 2007). Therefore, structural rearrangements of ribosomal complexes occurring on timescales faster than ~10 msec can lead to time-averaged values of E_{FRET}, making it difficult or impossible to confidently identify and investigate these conformational changes. Given that, *in vivo*, a single elongation cycle occurs on a timescale of ~50–200 msec at 37 °C (i. e. corresponding to a rate of ~5–20 amino acids per sec (Kennell and Riezman, 1977; Bremer and Dennis, 1987; Sorensen and Pedersen, 1991; Liang et al., 2000; Proshkin et al., 2010), with rate-limiting structural rearrangements of the elongating ribosomal complex expected to occur on timescales of a few msec to a couple hundred msec at 20–37 °C (Pape et al., 1998; Savelsbergh et al., 2003; Gromadski and Rodnina, 2004; Pan et al., 2007), it is perhaps inevitable that some subset of ribosomal complex dynamics will be poorly defined or even completely missed by TIRFM. Indeed, nearly all TIRFM-based smFRET studies of protein synthesis to date report at least one example of a conformational process that is missed due to time-averaged values of E_{FRET} (for a particularly clear example involving tRNA fluctuations within ribosomal complexes at low Mg^{2+} concentrations, see (Blanchard et al., 2004b)). In principle, the time resolution of smFRET experiments can be extended to a few μsec per timestep by replacing the TIRFM equipped with an EMCCD camera detector with a confocal fluorescence microscope equipped with an avalanche photodiode detector (Cornish and Ha, 2007). However, confocal microscopy is constrained in that it entails excitation and detection of a single ribosomal complex at a time, significantly increasing the amount of time required to collect datasets large enough to be statistically significant. Consequently, only a single example of a confocal microscopy-based smFRET experiment on ribosomal complexes has thus far been reported (Blanchard et al., 2004b).

An additional limitation of both TIRFM and confocal fluorescence microscopy is a restriction on the maximum concentration of fluorescence-labeled molecules that can be maintained within the microfluidic flowcell during smFRET experiments. As described in Section 2.4, the evanescent field produced in a TIRFM confines the excitation of fluorescence-labeled components to just a thin layer of buffer beyond the quartz-buffer interface. Using point-like illumination and detection, a confocal fluorescence microscope likewise confines the excitation of fluorescence-labeled components to a small (typically diffraction-limited) focal volume (Pawley, 2006). Despite this, concentrations of fluorescence-labeled components exceeding several tens of nM will substantially lower the signal-to-noise of both TIRFM and confocal fluorescence microscopy. Therefore, it remains difficult to perform smFRET experiments involving the delivery of physiologically relevant concentrations of fluorescence-la-

beled ribosomal subunits, tRNAs, or translation factors into the microfluidic flowcell. This limitation has been recently overcome through the development of so-called zero-mode waveguides (Levene et al., 2003; Moran-Mirabal and Craighead, 2008), which decrease the effective illumination volume by several orders of magnitude over that achieved by total internal reflection. This approach enables experiments to be conducted at near-physiological concentrations of fluorescence-labeled components (Uemura et al., 2010) (reviewed in the chapter by Uemura and Puglisi of this volume).

A third limitation of TIRFM, which also applies to confocal fluorescence microscopy and the use of zero-mode waveguides, is the potential ambiguity of smFRET data collected on systems with multiple donor-acceptor pairs (Hohng et al., 2004; Clamme and Deniz, 2005; Munro et al., 2010a). These experiments are challenging because the spectral overlap between the desired donor-acceptor pairs that is required to generate the desired FRET signals generally gives rise to unavoidable spectral overlap between alternative donor-acceptor pairs that can generate unwanted FRET signals. In order to avoid convoluting the desired FRET signals with unwanted FRET signals, care must therefore be taken in designing the labeling scheme such that the distances between unwanted donor-acceptor pairs remains large enough that their FRET efficiency is minimized or eliminated. Even if unwanted FRET signals can be minimized or eliminated, however, the significant spectral overlap between the desired donor-acceptor pairs that is required to generate the desired FRET signals opposes the spectral separation that is subsequently required to effectively separate the emitted fluorescence into the various individual donor and acceptor channels. Even careful optimization of the optical setup yields incompletely separated donor and acceptor fluorescence emissions with very low signal-to-noise ratios, invariably degrading the quality of the smFRET data to the point where it cannot be quantitatively analyzed without extensive and rigorous correction of the spectral bleedthrough among the various donor and acceptor channels.

2.6. Analysis of smFRET data

Technically detailed general procedures for the analysis of smFRET data have been recently described (Joo and Ha, 2007; Blanco and Walter, 2010) and a practical guide aimed at the non-expert is also available (Roy et al., 2008). Drawing from this framework, in this section we provide a brief summary of the steps involved in the analysis of complex smFRET data such as that obtained from smFRET studies of protein synthesis and highlight those aspects of these procedures which have the most impact on the analysis and interpretation of the data.

The first step in the analysis of smFRET data is to extract E_{FRET} *versus* time trajectories, or smFRET trajectories, from the digital video output of the EMCCD camera. This is a fairly straightforward step that is usually done using typically a semi- or fully automated procedure that involves: (i) identification of single fluorophores in the donor and acceptor images recorded by the EMCCD camera; (ii) alignment of the donor and acceptor images to generate superimposed single donor-acceptor pairs; (iii) plotting of donor and acceptor emission intensities *versus* time trajectories for each donor-acceptor pair; (iv) spectral bleedthrough correction of donor emission into the acceptor channel and, if necessary, acceptor emission into the donor channel; (v) baseline correction of the donor and acceptor emission intensities such that the background from the donor and acceptor channels following photobleaching average to zero intensity; and (vi) plotting of E_{FRET} *versus* time trajectories from the bleedthrough- and baseline-corrected donor and acceptor emission intensity *versus* time trajectories using the equation $E_{FRET} = I_A/(I_A + I_D)$, where I_A and I_D are the emission intensities of the acceptor and the donor, respectively.

At this point, only those trajectories that can be shown to arise from *bona fide* FRET between a single donor-acceptor pair are selected for further analysis. As this selection is typically based on visual inspection or a combination of semi-automated procedures and visual inspection, it is important to minimize user bias by defining a set of objective selection criteria. Because such criteria will be specific to each project and may vary across research groups, it is important that they be clearly reported in individual publications. Commonly applied criteria include requirements that: (i) the emission intensities of the donor and acceptor are within the intensity distributions expected for single donors and acceptors, respectively; (ii) the donor and acceptor undergo photobleaching in a single time step; and (iii) changes in donor and acceptor emission intensities are anti-correlated. For examples of selection criteria specific to smFRET studies of protein synthesis, see (Blanchard et al., 2004b; Munro et al., 2007; Wang et al., 2007; Cornish et al., 2008; Fei et al., 2008).

The detection of single fluorophores at the time resolutions common to smFRET experiments invariably leads to noisy raw smFRET trajectories. In order to avoid missing mechanistically important features obscured by the noisy nature of the data or, conversely, to avoid over- or misinterpreting noise as a mechanistically important feature of the data, statistically rigorous inference of the data should be performed. This is typically achieved by using a hidden Markov model to identify discrete conformational states within the noisy raw smFRET trajectories and to determine the most probable path (i. e. the idealized trajectory) through these conformational states (Qin et al., 1996; Andrec et al., 2003; McKinney et al., 2006; Talaga, 2007; Bronson et al., 2009; Liu et al., 2010). An important aspect of developing a hidden Markov model of a raw smFRET trajectory is determination of the model complexity (i. e. the number of conformational states that can be confidently inferred from the raw smFRET trajectory) and the model parameters (i. e. the distribution of E_{FRET} values and transition rates associated with each of the inferred conformational states). This is most commonly accomplished using maximum likelihood-based methods (Qin et al., 1996; McKinney et al., 2006; Liu et al., 2010) which seek to find the parameters that maximize the probability of the data given the model. These methods have a tendency to overestimate the model complexity, however, often leading to problems with overfitting of the data (Bronson et al., 2009; Liu et al., 2010). Thus, care should be taken in identifying additional (i. e. intermediate) conformational states using maximum likelihood-based hidden Markov modeling of smFRET trajectories; ideally, the authenticity of intermediate states identified in this way should be verified though structural and/or biochemical studies. More recently, an alternative to maximum likelihood, termed maximum evidence, has been suggested for the analysis of smFRET trajectories (Bronson et al., 2009). This method, which seeks to find the model that maximizes the probability of the data, naturally avoids overfitting and can have a significantly lower tendency to overestimate the number of conformational states that can be confidently identified in the raw smFRET trajectories.

Further analysis of the raw smFRET trajectories and/or idealized trajectories is highly dependent on the experimental question that is being addressed by the smFRET experiment (Roy et al., 2008). In general, however, equilibrium properties of the system can be derived from the population distribution of observed values of E_{FRET} over a large number of individual smFRET trajectories. The rates of transition between the various conformational states of a system that is in a dynamic conformational equilibrium can be obtained from exponential fits to the distribution of dwell times spent at each conformational state before transitioning to each of the other conformational states (Colquhoun and Hawkes, 1995) or by using the transition probability matrix that results directly from hidden Markov model analysis (McKinney et al., 2006). Non-equilibrium properties of the system can be assessed by monitoring the evolution of E_{FRET} as a function of time for a reaction in which a substrate or ligand is stopped-flow delivered to a surface-tethered biomolecule of interest (Blanchard et al., 2004a). (1319)

3. smFRET studies of the translocation step of translation elongation

3.1. Translocation of the mRNA-tRNA complex through the ribosome

During the elongation stage of protein synthesis, the ribosome sequentially adds amino acids to a growing polypeptide chain at a rate of ~10–20 amino acids sec^{-1} at 37 °C *in vivo* (Kennell and Riezman, 1977). With the addition of each amino acid, the ribosome repetitively cycles through three major steps: aminoacyl-tRNA (aa-tRNA) selection (Rodnina et al., 2005), peptide bond formation (Beringer and Rodnina, 2007), and translocation (Shoji et al., 2009). Upon accommodation of an aa-tRNA into the ribosomal A (aa-tRNA binding) site at the end of aa-tRNA selection, peptide bond formation results in the transfer of the nascent polypeptide from the peptidyl-tRNA at the ribosomal P (peptidyl-tRNA binding) site to the A-site aa-tRNA. The resulting ribosomal pre-translocation (PRE) complex is the substrate on which the GTPase elongation factor G (EF-G) will act to catalyze translocation by precisely one codon. During translocation, the newly deacylated tRNA at the P site moves into the ribosomal E (exit) site, the newly formed peptidyl-tRNA at the A site moves into the P site, and the next mRNA codon moves into the A site. The resulting ribosomal post-translocation (POST) complex is now ready to participate in aa-tRNA selection during the next round of the elongation cycle. How the ribosome accomplishes the rapid and precise movement of the mRNA-tRNA complex during translocation continues to be the subject of intense investigation using genetic, biochemical, structural, and, most recently, smFRET approaches

(reviewed in (Shoji et al., 2009; Aitken et al., 2010; Dunkle and Cate, 2010; Frank and Gonzalez, 2010).

3.2. Structural rearrangements of the translational machinery important for translocation

Based on the ribosome's universally conserved two-subunit architecture, Spirin (Spirin, 1968) and Bretscher (Bretscher, 1968) were the first to hypothesize that translocation proceeds *via* an intermediate configuration of the tRNAs within the PRE complex that is somehow coupled to a relative rearrangement of the small (30S in *Escherichia coli*) and large (50S in *E. coli*) ribosomal subunits. Experimental validation of this hypothesis first came from chemical probing studies (Moazed and Noller, 1989), subsequently confirmed by ensemble FRET experiments (Odom et al., 1990), demonstrating that peptide bond formation results in the spontaneous rearrangement of the ribosome-bound tRNAs from their "classical" P/P (denoting the 30S P/50S P sites) and A/A configurations, into intermediate "hybrid" P/E and A/P configurations. As the naming convention suggests, in their hybrid configurations the aminoacyl acceptor ends of the P- and A-site tRNAs have moved into the 50S subunit E and P sites, respectively, while their anticodon stem-loops remain bound at the 30S subunit P and A sites. EF-G likely promotes further rearrangements of the aminoacyl acceptor end of the A-site peptidyl-tRNA within the 50S subunit P site (Borowski et al., 1996; Pan et al., 2007) and subsequently catalyzes the movement of the tRNA anticodon stem-loops and the associated mRNA from the 30S subunit P and A sites into the 30S subunit E and P sites, respectively, thus completing the translocation reaction.

A decade after the chemical modification studies, cryogenic electron microscopic (cryo-EM) reconstructions of PRE complex analogs containing vacant A sites (PRE^{-A} complexes) and stabilized through the binding of EF-G in the presence of GDPNP, a non-hydrolyzable GTP analog, allowed visualization of the P/E tRNA configuration and of possibly associated large-scale conformational rearrangements of the PRE^{-A} complex (Frank and Agrawal, 2000; Valle et al., 2003). Comparison of cryo-EM reconstructions of PRE^{-A} complexes in the presence and absence of EF-G(GDPNP) revealed three major conformational changes. These were: (i) the aforementioned movement of the deacylated P-site tRNA from the P/P to the P/E configuration; (ii) the ~20 Å movement of a universally conserved and highly dynamic domain of the 50S subunit E site, the L1 stalk, from an open to a closed conformation such that it establishes a direct interaction with the central fold, or elbow, domain of the P/E-configured tRNA; and (iii) the counter-clockwise, ratchet-like rotation of the 30S subunit with respect to the 50S subunit (when viewed from the solvent side of the 30S subunit) from a non-rotated to a rotated subunit orientation.

Hereafter we will refer to the two conformations of the PRE^{-A} complex observed in the cryo-EM studies described above as global state 1 (GS1), observed in the absence of EF-G(GDPNP) and encompassing non-rotated subunits, classically bound tRNAs, and an open L1 stalk, and global state 2 (GS2), observed in the presence of EF-G(GDPNP) and encompassing rotated subunits, hybrid-bound tRNAs, and a closed L1 stalk (Figure 3). We note that analogous terms have been introduced by Frank and co-workers (Macro State I and Macro State II (Frank et al., 2007)), Noller and co-workers (non-rotated/classical and rotated/hybrid (Ermolenko et al., 2007b)), and Cate and co-workers (R_0 and R_F (Zhang et al., 2009)). Regardless of the differing terminologies, as originally hypothesized by Spirin and Bretscher, the conformational changes of the ribosome and the ribosome-bound tRNAs encompassed by the GS1-to-GS2 transition are expected to play a major role in facilitating the translocation reaction. Indeed, biochemical evidence lends support to the notion that GS2 represents an authentic on-pathway translocation intermediate (Dorner et al., 2006; Horan and Noller, 2007).

Using the available crystal and cryo-EM structures as guides, numerous donor-acceptor labeling schemes have been developed to investigate the dynamics of ribosome and tRNA conformational changes within PRE and PRE^{-A} complexes by smFRET, a subset of which will be discussed here. smFRET between A- and P-site tRNAs labeled within their elbow regions was initially shown to report on the occupancy of the classical and hybrid tRNA binding configurations (Blanchard et al., 2004b). Movement of the L1 stalk from an open to a closed conformation has been tracked through smFRET between donor and acceptor fluorophores attached to ribosomal proteins L1 and L9 (Fei et al., 2009) (an alternative L1-L33 smFRET signal has also been used for this purpose in an independent study (Cornish et al., 2009)). In the closed conformation, the L1 stalk can form intermolecular contacts with the elbow domain of the P/E-configured tRNA;

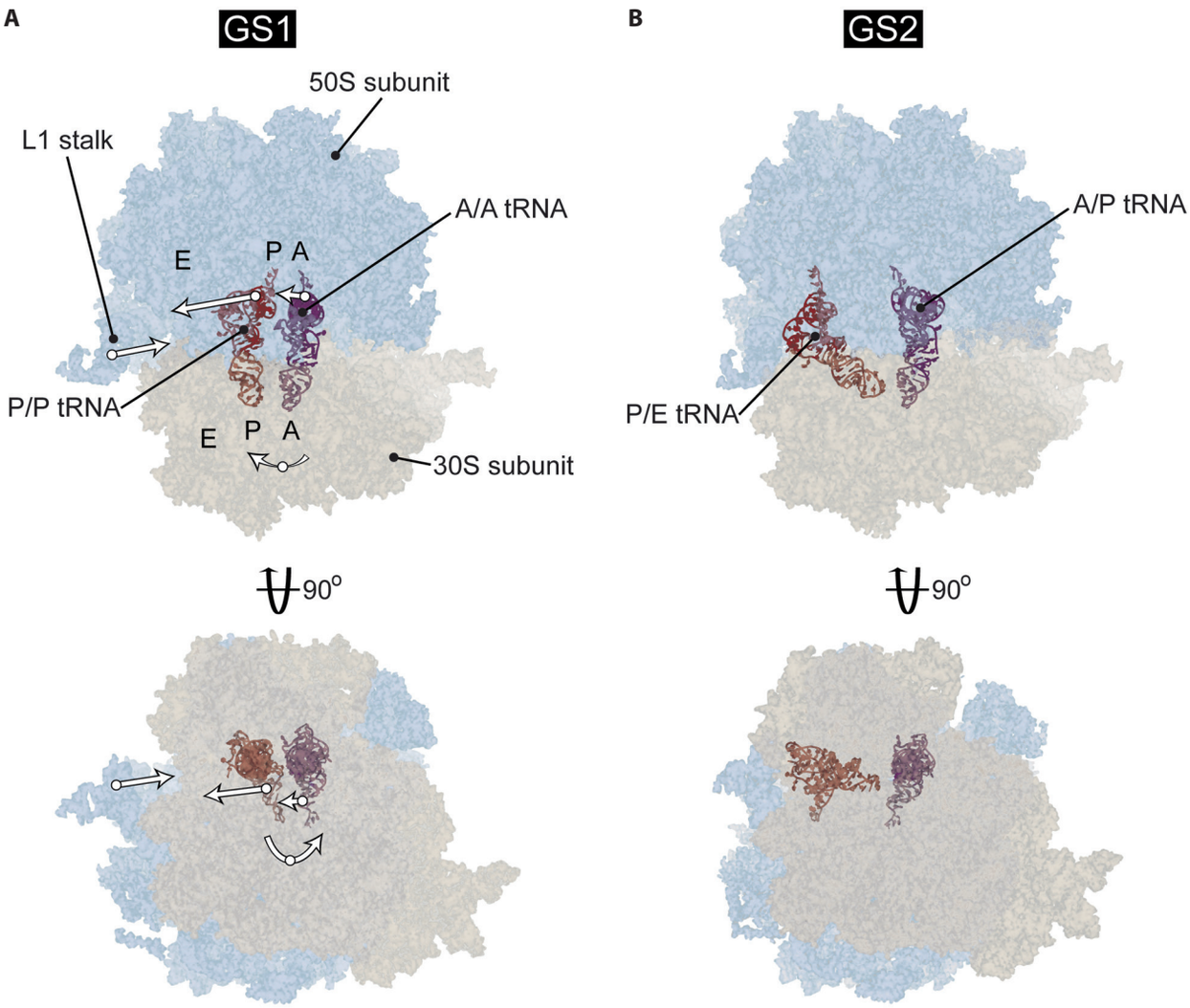

Fig. 3 Structural models of the GS1 and GS2 states of the PRE complex. Structural models were generated by flexible-fitting of atomic resolution structures into cryo-EM maps using molecular dynamics (Agirrezabala et al., 2008; Trabuco et al., 2008) kindly provided by Joachim Frank. The 30S and 50S ribosomal subunits were rendered in semi-transparent space-filling representations such that the P- and A-site tRNAs bound within the inter-subunit space and rendered in cartoon representations could be clearly visualized. Shown are perspectives from a side-view of the PRE complex illustrating the E-, P-, and A-tRNA binding sites (top row) as well as a view from the solvent-accessible surface of the 30S subunit (bottom row), obtained by 90' rotation of the side-view so that the 50S subunit is now behind the visual plane. (A) The GS1 state encompasses classically bound tRNAs, an open L1 stalk, no interaction between the L1 stalk and the P/P-configured tRNA, and a non-rotated subunit orientation. The white arrows mark the relative directions in which the tRNAs and the L1 stalk move and the 30S subunit rotates with respect to the 50S subunit during the transition from the GS1 state to the GS2 state. (B) The GS2 state encompasses hybrid-bound tRNAs, a closed L1 stalk, an interaction between the L1 stalk and the P/E-configured tRNA, and a rotated subunit orientation.

an smFRET signal between fluorophore-labeled L1 and P-site tRNA was developed to report on the formation and disruption of these contacts (Fei et al., 2008) (a similar L1-tRNA smFRET signal has also been used for this purpose in an independent study (Munro et al., 2010a)). Finally, inter-subunit rotation has been monitored through smFRET signals developed by reconstituting donor- and acceptor-labeled ribosomal proteins into 30S and 50S subunits; results obtained with an S6-L9 smFRET signal will be described below (Ermolenko et al., 2007a; Cornish et al., 2008). An additional inter-subunit FRET signal has been developed by hybridizing fluorescence-labeled oligonucleotides to helical extensions engineered into helix 44 of 16S ribosomal RNA (rRNA) within the 30S subunit and helix 101 of 23S rRNA within the 50S subunit (Dory-

walska et al., 2005; Marshall et al., 2008). This latter signal, however, seems insensitive to the inter-subunit rotation observed by cryo-EM, instead reporting on an as yet undefined inter-subunit conformational switch that is uniquely triggered upon deacylation of the P-site tRNA *via* peptide bond formation and uniquely reset upon translocation of the A-site peptidyl-tRNA into the P site (Marshall et al., 2008; Aitken and Puglisi, 2010; Frank and Gonzalez, 2010).

Steady-state smFRET experiments on POST complexes prepared using the donor-acceptor pairs described above predominantly yield smFRET trajectories that stably sample a single FRET state with a distinct value of E_{FRET}, with the exception of the L1-L9 and the L1-L33 pairs. The specific dynamics of the L1-L9 and L1-L33 smFRET signals within a particular POST complex instead depend on the presence and identity of the E-site tRNA. Collectively, the data suggest that, prior to aa-tRNA accommodation into the A site and peptide bond formation, POST complexes primarily exist in a stable GS1-like structural state in which: (i) tRNAs exhibit a strong preference for their classical configurations; (ii) the L1 stalk primarily favors either the open conformation or a half-closed conformation that is unique to POST complexes carrying an E-site tRNA; (iii) interactions between the L1 stalk and the P-site tRNA are not made; and (iv) the majority of ribosomes are fixed in the non-rotated subunit orientation.

Deacylation of the P-site peptidyl-tRNA *via* peptidyl transfer to either aa-tRNA or the antibiotic puromycin at the A site yields PRE and PRE^{-A} complexes, respectively. Puromycin, which mimics the aminoacyl end of aa-tRNA, binds at the 50S A site and participates in peptide bond formation, ultimately dissociating from the 50S A site and leaving deacylated tRNA at the P site (Traut and Monro, 1964). In the absence of EF-G, the majority of steady-state smFRET experiments on PRE/PRE^{-A} complexes prepared using the donor-acceptor pairs described above yield smFRET trajectories that stochastically fluctuate between two FRET states with distinct values of E_{FRET} (Figure 4). In all cases, one of the observed FRET states could be assigned to GS1, the second to GS2. Taken together, these experiments strongly suggest that, upon peptide bond formation and in the absence of EF-G, the entire PRE complex can stochastically fluctuate between GS1 and GS2, using the surrounding thermal bath as its sole energy source.

PRE/PRE^{-A} complexes therefore provide an excellent example of a dynamically heterogeneous system. In an ensemble FRET experiment the asynchronous transitioning of individual PRE or PRE^{-A} complexes between GS1 and GS2 would be expected to yield a single, population-averaged value of E_{FRET}; indeed, such population-averaged values of E_{FRET} based on ensemble FRET experiments using several of the donor-acceptor pairs described above have been reported (Johnson et al., 1982; Paulsen et al., 1983; Odom et al., 1990; Ermolenko et al., 2007a; Ermolenko et al., 2007b). By eliminating this population averaging, the smFRET experiments: (i) reveal that PRE/PRE^{-A} complexes exist in a dynamic conformational equilibrium, fluctuating stochastically between GS1 and GS2; (ii) allow dissection of individual smFRET trajectories into time intervals spent in the GS1 or GS2 states, so identified by their characteristic values of E_{FRET}; (iii) enable detailed thermodynamic and kinetic characterization of the individual GS1 and GS2 states; and, as we shall see below, (iv) open the door to a still unfolding series of studies into the role that thermally activated structural fluctuations of the PRE complex may play in the mechanism and regulation of translocation.

Strong support for the interpretation of the smFRET data presented above has come from two ensemble FRET studies in which the S6-L9 FRET signal was used to monitor inter-subunit rotation as a function of experimental conditions favoring either the classical or hybrid tRNA configurations (Ermolenko et al., 2007a; Ermolenko et al., 2007b). These ensemble experiments showed that inter-subunit rotation in PRE/PRE^{-A} complexes can indeed occur in the absence of EF-G and demonstrated that PRE/PRE^{-A} ribosomes can be stabilized in the non-rotated or rotated subunit orientations by imposing experimental conditions that favor the classical or hybrid tRNA configurations, respectively. These data strongly suggest that the non-rotated subunit orientation is thermodynamically favored when the tRNAs are in the classical configuration (i. e. the GS1 state), while the rotated subunit orientation is thermodynamically favored when the tRNAs are in the hybrid configuration (i. e. the GS2 state). In complete agreement with this view, two recent cryo-EM studies in which particle classification methods were applied to a PRE complex revealed the existence of two classes of particles with structures corresponding to GS1 and GS2 (Agirrezabala et al., 2008; Julian et al., 2008).

The results of the smFRET and ensemble FRET experiments described above demonstrate that access to GS2 – and thus forward progression along the translocation reaction coordinate – can occur in the absence of EF-G and GTP hydrolysis. Indeed, full

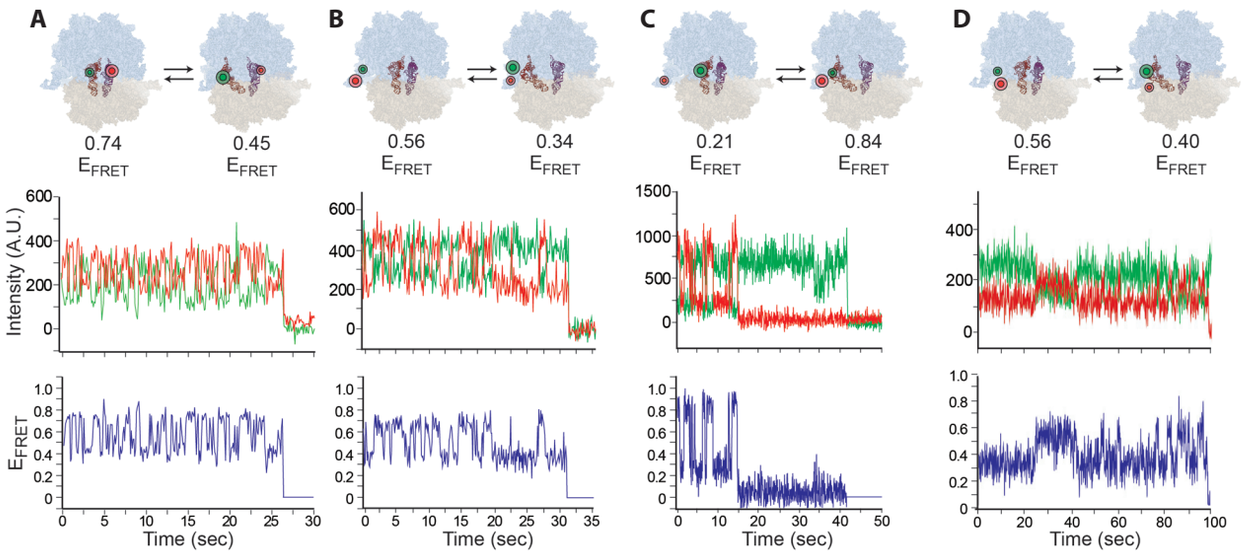

Fig. 4 E_{FRET} *versus* time trajectories derived from PRE complexes undergoing thermally activated fluctuations between GS1 and GS2. Structural models of GS1 and GS2 (top row) are displayed as in the top row of Figure 3. The approximate positions of the donor and acceptor fluorophores corresponding to each donor-acceptor labeling scheme are shown as green and red spheres, respectively. Representative donor and acceptor emission intensities *versus* time trajectories (middle row) are shown in green and red, respectively. The corresponding E_{FRET} *versus* time trajectories (bottom row), calculated using $E_{FRET} = I_A / (I_A + I_D)$, where I_A and I_D are the emission intensities of the acceptor and the donor, respectively, are shown in blue. (A) The tRNA-tRNA smFRET signal fluctuates between 0.74 (classical tRNA configuration, GS1) and 0.45 (hybrid tRNA configuration, GS2) values of E_{FRET} (Adapted from (Blanchard et al., 2004b) with permission from The National Academy of Sciences, USA). (B) The L1-L9 smFRET signal fluctuates between 0.56 (open L1 stalk conformation, GS1) and 0.34 (closed L1 stalk conformation, GS2) values of E_{FRET} (Reprinted from (Fei et al., 2009) with permission from The National Academy of Sciences, USA). (C) The L1-tRNA smFRET signal fluctuates between 0.21 (open L1 stalk not interacting with P/P-configured tRNA, GS1) and 0.84 (closed L1 stalk interacting with P/E-configured tRNA, GS2) values of E_{FRET} (Reprinted from (Fei et al., 2008) with permission from Elsevier). (D) The S6-L9 inter-subunit smFRET signal fluctuates between 0.56 (non-rotated subunit orientation, GS1) and 0.40 (rotated subunit orientation, GS2) values of E_{FRET}. (Adapted from (Cornish et al., 2008) with permission from Elsevier).

rounds of spontaneous translation elongation have been observed in vitro in a factor-free environment, in which the ribosome moves slowly but directionally along the mRNA template to generate polypeptides of defined length (Pestka, 1969; Gavrilova and Spirin, 1971; Gavrilova et al., 1976). It seems, therefore, that many, if not all, of the conformational rearrangements required for translocation can be accessed with the input of thermal energy alone. The fluctuations of PRE/PRE^{-A} complexes observed by smFRET represent dynamic events that are likely important for promoting the movement of the mRNA-tRNA complex during translocation; these fluctuations may thus increase the probability that spontaneous translocation will occur.

3.3. Identification and characterization of intermediate states connecting GS1 and GS2

The tRNA and ribosome structural rearrangements that constitute transitions between GS1 and GS2 are undoubtedly complex, involving significant local and global reconfigurations of ribosome-ribosome and ribosome-tRNA interactions (Korostelev et al., 2008). Despite this complexity, however, the majority of smFRET studies to date report fluctuations between just two major FRET states corresponding to GS1 and GS2. Since individual transitions between GS1 and GS2 must necessarily occur *via* some pathway (or, more likely, *via* any one of numerous parallel pathways), the failure of the majority of smFRET studies to identify any intermediate states connecting GS1 and GS2 most likely arises from either (i) the limited time resolution (typically 25–100 msec per frame in studies of ribosome and tRNA dynamics) with which TIRFM-based smFRET studies can resolve energetically unstable,

and thus transiently sampled, intermediate states or (ii) the limited sensitivity with which a specific donor-acceptor pair can be used to detect the distance change associated with the formation of a particular intermediate state. It may therefore be necessary to perform smFRET experiments using higher time resolution confocal microscopy (up to several μsec per frame) (Cornish and Ha, 2007) and/or alternative donor-acceptor labeling schemes in order to capture intermediate states that may exist on the pathway(s) connecting GS1 and GS2.

Despite the failure of most of the smFRET studies of PRE/PRE^{-A} complexes to detect any intermediate states, two studies have used maximum likelihood-based hidden Markov modeling of smFRET trajectories to identify an intermediate FRET state using a tRNA-tRNA smFRET signal (Munro et al., 2007) and two intermediate FRET states using an L1 stalk-tRNA smFRET signal (Munro et al., 2010a). Structurally, the tRNA-tRNA intermediate FRET state has been assigned to a PRE complex containing P/E- and A/A-configured tRNAs, an intermediate configuration which had been previously proposed on the basis of tRNA mutagenesis experiments (Pan et al., 2006) and ensemble kinetic experiments (Pan et al., 2007) based on a previously established kinetic scheme of translocation (Savelsbergh et al., 2003). Contrasting with the tRNA-tRNA intermediate FRET state, the two intermediate L1-tRNA FRET states remain to be structurally or biochemically characterized. A somewhat surprising feature of the tRNA-tRNA and L1-tRNA intermediate FRET states that have been thus far identified is that, in all cases, their equilibrium populations are greater than that of the FRET state assigned to GS2, implying that the thermodynamic stabilities of the intermediate states are actually greater than that of GS2. We anticipate that identification of these new intermediate states will continue to drive structural, biochemical, and smFRET studies aimed at elucidating the physical basis underlying transitions between GS1 and GS2.

3.4. Allosteric regulation of the GS1/GS2 dynamic equilibrium

Using the tRNA-tRNA, L1-L9 (or L1-L33), L1-tRNA, and S6-L9 inter-subunit smFRET signals, numerous studies have demonstrated that both the equilibrium distributions of FRET states corresponding to GS1 and GS2 as well as the rates of transitions between these FRET states are highly sensitive to experimental conditions. These include the concentration of Mg^{2+} ions, the absence, presence, identity, and acylation state of the tRNAs, the absence or presence of translation factors, and the absence or presence of antibiotics targeting the ribosome. Assuming that the conformational changes associated with the GS1-to-GS2 transition are a fundamental part of the translocation mechanism and that GS2 is an obligatory intermediate on the translocation pathway, these observations suggest that specific control over the dynamics of the PRE ribosome, through the acceleration/deceleration of conformational changes and the associated stabilization/destabilization of specific conformational states, could provide an effective means for regulating the translocation reaction. In this view, ribosomal ligands may function by rectifying the intrinsic conformational dynamics of the PRE complex in order to promote or inhibit the translocation reaction. Indeed, as described below, modulation of PRE complex dynamics through changes in experimental conditions can often be strongly correlated with the effect of those changes on the rate of translocation.

The dynamic exchange of tRNAs between classical and hybrid configurations necessarily requires the remodeling of multiple tRNA-rRNA and tRNA-ribosomal protein interactions; this suggests that the classical/hybrid tRNA equilibrium may be modulated by the concentration of Mg^{2+} ions in solution, since Mg^{2+} is known to play a crucial role in the folding and stabilization of RNA structures (Draper, 2004). An investigation of the Mg^{2+} dependence of a tRNA-tRNA smFRET signal over a range of 3.5 to 15 mM Mg^{2+} within a PRE complex carrying deacylated $tRNA^{fMet}$ at the P site and a peptidyl-$tRNA^{Phe}$ analog, *N*-acetyl-Phe-$tRNA^{Phe}$, at the A site revealed a Mg^{2+}-dependent shift in the equilibrium distribution of classical and hybrid configurations (Kim et al., 2007). Specifically, at low concentrations of Mg^{2+} (3.5 mM) the hybrid configuration is favored. However, the equilibrium fraction of the classical configuration increases with increasing Mg^{2+}, with the classical and hybrid configurations becoming equally populated at ~4 mM Mg^{2+}. Analysis of the transition rates between classical and hybrid configurations revealed that this occurs primarily through a Mg^{2+}-dependent stabilization of the classical configuration that decreases the rate of classical-to-hybrid tRNA transitions while leaving the rate of hybrid-to-classical tRNA transitions unaffected. In structural terms, this is interpreted to mean that classically bound tRNAs form a more extensive and compact network of Mg^{2+}-stabilized tRNA-rR-

NA and/or tRNA-ribosomal protein interactions. At higher Mg^{2+} concentrations (~7 mM and above), the classical configuration is almost exclusively favored on account of the decreased rate of classical-to-hybrid transitions. These results correlate strongly with – and offer a mechanistic explanation for – the known inhibitory and stimulatory effects, respectively, of high and low Mg^{2+} concentration on the rate of translocation. At high Mg^{2+} concentrations (~30 mM), translocation is blocked almost entirely, even in the presence of EF-G (Spirin, 1985), which can be rationalized by a Mg^{2+}-induced stalling of the classical-to-hybrid tRNA transition evidenced by smFRET. At the other extreme of low Mg^{2+} (~3 mM), spontaneous translocation can proceed rapidly (Spirin, 1985), an effect presumably linked to the accelerated rate of the classical-to-hybrid transition under low-Mg^{2+} conditions. smFRET evidence thus suggests that perturbations to the rate of the classical-to-hybrid tRNA transition can affect the rate of translocation, implying that manipulation of the GS1-to-GS2 transition may serve to regulate this critical step in protein synthesis.

Changes in the acylation state and identity of the P- and A-site tRNAs within ribosomal elongation complexes have similarly been found to influence the energetics of ribosome and tRNA conformational fluctuations. As discussed above, the presence of a peptide on the P-site tRNA largely suppresses ribosome and tRNA dynamics within a POST complex, whereas PRE/PRE^{-A} complexes bearing a deacylated P-site tRNA exhibit pronounced ribosome and tRNA dynamics. In addition, PRE/PRE^{-A} complex dynamics have been shown to be sensitive to the identity of the P-site tRNA. For example, a comparison of inter-subunit rotation dynamics within four different PRE^{-A} complexes differing only in the identity of the deacylated P-site tRNA ($tRNA^{fMet}$, $tRNA^{Phe}$, $tRNA^{Tyr}$, and $tRNA^{Met}$ were used), revealed distinct thermodynamic and kinetic parameters underlying reversible inter-subunit rotation (Cornish et al., 2008). Likewise, PRE^{-A} complexes containing either $tRNA^{fMet}$ or $tRNA^{Phe}$ at the P site exhibit differences in the rate of L1 stalk and L1 stalk-P-site tRNA interaction dynamics that mirror those observed in the inter-subunit rotation experiments (Fei et al., 2008; Cornish et al., 2009; Fei et al., 2009; Munro et al., 2010a). Different P-site tRNA species, therefore, make sufficiently unique contacts with the ribosome such that they influence large-scale structural rearrangements of the PRE/PRE^{-A} ribosome in distinct ways. Similarly, the presence and acylation state of the A-site tRNA appears to influence the thermodynamic and kinetic behavior of conformational equilibria monitored by the individual smFRET signals. For example, the presence of A-site dipeptidyl-tRNA *versus* aa-tRNA increases the population of the hybrid tRNA configuration by increasing the rate of classical-to-hybrid tRNA transitions, as monitored by tRNA-tRNA smFRET (Blanchard et al., 2004b). Likewise, using the L1-tRNA smFRET signal, addition of aa-tRNA to PRE^{-A} complexes caused a slight increase in the rate with which the L1 stalk-P/E tRNA interaction is formed, with minimal effect on the rate with which this interaction is disrupted; occupancy of the A site by a tripeptidyl-tRNA increased the forward rate by an additional 6-fold, again with minimal effect on the reverse rate (Fei et al., 2008). Finally, the presence of a peptidyl-tRNA at the A site of PRE complexes shifts the equilibrium from the open to the closed L1 stalk conformation, as monitored by the L1-L9 smFRET signal, primarily by accelerating the rate of the open-to-closed L1 stalk transition (Fei et al., 2009).

From the data discussed above, a picture begins to emerge in which large-scale conformational rearrangements of the entire PRE complex can be rectified and allosterically controlled through even subtle and highly localized changes in interactions between the ribosome and its ligands (i. e. the presence of dipeptidyl- *versus* aa-tRNA at the A site). This feature of the PRE complex has apparently been exploited by antibiotics targeting the ribosome which often function by inhibiting the dynamics of the translational machinery. Indeed, smFRET studies have provided evidence that translocation inhibitors specifically interfere with the conformational dynamics of the PRE complex. For example, the potent translocation inhibitor viomycin, which binds at the interface between the 30S and 50S subunits (Yamada et al., 1978; Moazed and Noller, 1987; Johansen et al., 2006; Stanley et al., 2010), has been shown by smFRET to almost exclusively stabilize the rotated subunit orientation of the PRE complex, consistent with previous ensemble studies (Ermolenko et al., 2007b), and to almost completely suppress transitions between the rotated and non-rotated subunit orientations (Cornish et al., 2008). Interestingly, while chemical probing experiments suggest that viomycin stabilizes the P/E configuration of the P-site tRNA (Ermolenko et al., 2007b), tRNA-tRNA smFRET experiments suggest that viomycin instead decreases the rate of fluctuations between the classical and hybrid tRNA configurations, with conflicting results on whether the classical or hybrid configurations of the tRNAs are stabilized (Kim et al., 2007; Feldman et al., 2010).

smFRET investigations of PRE complexes have also been conducted in the presence of a collection of aminoglycoside antibiotics (Feldman et al., 2010), drugs that bind to helix 44 within 16S rRNA, stabilizing a conformation of the universally conserved 16S rRNA nucleotides A1492 and A1493 in which they are displaced from helix 44, adopting extra-helical positions that allow them to interact directly with the codon-anticodon minihelix at the 30S A site (Carter et al., 2000). All of the aminoglycosides tested were shown to suppress tRNA dynamics, specifically decreasing the rate of transitions out of the classical tRNA configuration and thus driving a net stabilization of the classical configuration. Although the observed effects are small (~1.5-fold rate decreases corresponding to ~1.7fold increases in the stability of the classical tRNA configuration, on average), the magnitude of these effects elicited by each of the aminoglycosides tested correlates with the reduction in translocation rate observed in the presence of each drug (Peske et al., 2004; Feldman et al., 2010). Therefore, inhibition of transitions into the hybrid state and the resulting stabilization of the classical state represent a general mechanism for translocation inhibition by aminoglycosides, with subtle differences in the chemical structure of the antibiotic dictating the degree of inhibition. Taken together, the viomycin and aminoglycoside studies discussed above illustrate that inhibition of ribosome and/or tRNA dynamics within the PRE complex represents a general inhibition strategy leveraged by a variety of antibiotics targeting the ribosome.

3.5. EF-G-mediated control of the GS1/GS2 dynamic equilibrium during translocation

Perhaps the most dramatic effect on ribosome and tRNA dynamics within PRE/PRE^{-A} complexes is elicited by EF-G. smFRET studies have revealed that binding of EF-G(GDPNP) to PRE^{-A} complexes leads to stabilization of all structural features characterizing GS2: ribosomal subunits are stabilized in their rotated orientation, the L1 stalk is stabilized in the closed conformation, and the P-site tRNA is stabilized in its P/E configuration, where it forms a long-lived intermolecular interaction with the L1 stalk (Cornish et al., 2008; Fei et al., 2008; Cornish et al., 2009; Fei et al., 2009; Munro et al., 2010b) (Figure 5). Particularly remarkable is the stabilization of the closed state of the L1 stalk, which demonstrates that binding of EF-G(GDPNP) to the ribosome's GTPase factor binding site can allosterically regulate L1 stalk dynamics ~175 Å away at the ribosomal E site. A major role of EF-G therefore appears to be its ability to bias intrinsic conformational fluctuations of the ribosome and tRNAs towards the on-pathway translocation intermediate GS2. In accord with the ability of the ribosome to translocate either in the forward (Pestka, 1969; Gavrilova and Spirin, 1971; Gavrilova et al., 1976; Bergemann and Nierhaus, 1983) or reverse (Shoji et al., 2006; Konevega et al., 2007) directions in the absence of EF-G, one of EF-G's main mechanistic functions may be to stabilize GS2, preventing reverse fluctuations along the translocation reaction coordinate and thus guiding the directionality of a process that the ribosome is inherently capable of coordinating on its own. This model finds strong support from biochemical experiments demonstrating that EF-G(GDPNP) stimulates the rate of translocation ~1,000-fold relative to uncatalyzed spontaneous translocation, and that GTP hydrolysis in the EF-G(GTP)-catalyzed reaction provides an additional rate enhancement of only ~50-fold (Rodnina et al., 1997; Katunin et al., 2002). GTP hydrolysis, which, based on fast kinetics measurements, precedes any further rearrangements of the aminoacyl acceptor end of the A-site peptidyl-tRNA within the large subunit P site (Borowski et al., 1996; Pan et al., 2007) as well as the movement of the mRNA-tRNA duplex on the small subunit, likely leads to conformational changes in EF-G as well as additional conformational changes of the PRE complex that promote these steps of the translocation reaction (Rodnina et al., 1997; Katunin et al., 2002; Savelsbergh et al., 2003).

Completion of the translocation reaction converts the PRE complex into a POST complex in which non-rotated subunits and classical tRNA configurations characteristic of GS1 prevail, and ribosome and tRNA dynamics are suppressed (Cornish et al., 2008; Fei et al., 2008). This effect has been observed in real time through pre-steady state smFRET experiments in which EF-G(GTP) was stopped-flow delivered to PRE complexes labeled with the inter-subunit S6-L9 smFRET pair (Cornish et al., 2008). Each PRE complex exhibits fluctuations between the non-rotated and rotated subunit orientations until the delivery of EF-G(GTP), at which point EF-G(GTP) binds to the PRE complex, catalyzes full translocation, and converts the PRE complex into a POST complex, thereby stabilizing the non-rotated subunit orientation. Similar pre-steady state smFRET experiments have been performed by stopped-flow delivery of an EF-Tu(GTP)aa-tRNA ternary complex and EF-G(GTP) to a POST complex

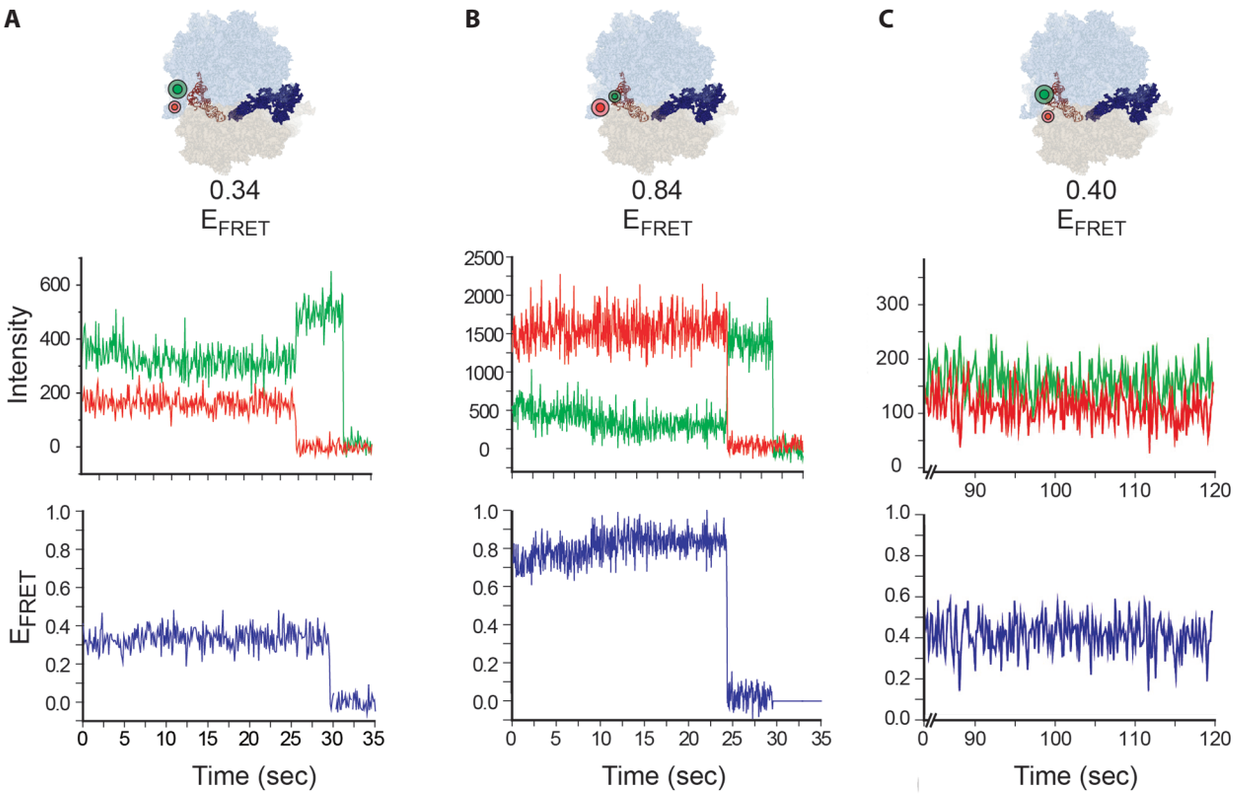

Fig. 5 E_{FRET} *versus* time trajectories derived from PRE^{-A} complexes stabilized in GS2 through their interactions with EF-G(GDPNP). A structural model of EF-G(GDPNP) bound to a PRE^{-A} complex (top row) generated by flexible-fitting of atomic resolution structures into a cryo-EM map using molecular dynamics was kindly provided by Joachim Frank. In this model, EF-G(GDPNP) was rendered in a space-filling representation and is shown in blue. The approximate positions of the donor and acceptor fluorophores corresponding to the three donor-acceptor labeling schemes are shown as green and red spheres, respectively. Donor and acceptor emission intensities *versus* time trajectories (middle row) and E_{FRET} *versus* time trajectories (bottom row) are shown as in Figure 4. (A) The L1-L9 smFRET signal is stabilized at the 0.34 (closed L1 stalk conformation, GS2) value of E_{FRET} (Reprinted from (Fei et al., 2009) with permission from The National Academy of Sciences, USA). (B) The L1-tRNA smFRET signal is stabilized at the 0.84 (closed L1 stalk interacting with P/E-configured tRNA, GS2) value of E_{FRET} (Reprinted from (Fei et al., 2008) with permission from Elsevier). (C) The S6-L9 inter-subunit smFRET signal is stabilized at the 0.40 (rotated subunit orientation, GS2) value of E_{FRET} (Adapted from (Cornish et al., 2008) with permission from Elsevier). Note that the analogous experiment using a tRNA-tRNA smFRET signal cannot be performed due to the opposing requirements for the presence of an A-site tRNA within a PRE complex in order to generate the smFRET signal and the absence of an A-site tRNA within a PRE^{-A} complex to establish stable binding of EF-G(GDPNP).

bearing fluorophore-labeled L1 and P-site peptidyl-tRNA. Stopped-flow delivery thus allows a full elongation cycle of aa-tRNA selection, peptidyl transfer, and EF-G(GTP)-catalyzed translocation to be monitored in real time using the L1-tRNA smFRET signal. The resulting smFRET trajectories exhibit a sharp transition from a low FRET state to a high FRET state upon peptidyl transfer (corresponding to formation of the intermolecular contacts between the L1 stalk and the P/E tRNA), followed by stable occupancy of the high FRET state until fluorophore photobleaching. This is in contrast to the analogous experiment performed in the absence of EF-G(GTP), where the initial transition from the low FRET state to the high FRET state is followed by fluctuations between the two FRET states (corresponding to repetitive formation and disruption of L1-tRNA contacts). These results suggest that during EF-G(GTP)-catalyzed translocation, the intermolecular interactions formed between the L1 stalk and the P/E-configured tRNA are maintained during the movement of the deacylated tRNA from the hybrid P/E configuration into the classical E/E configuration. Formation and maintenance of these interactions provides a molecular rationale to help explain how the L1 stalk facilitates the translocation reaction (Subramanian and Dabbs, 1980).

3.6. Translation factors direct thermally activated conformational processes throughout all stages of protein synthesis

In the previous sections we have described how the conformational dynamics of the ribosome and its tRNA substrates are modulated during the translocation step of the elongation cycle, providing a regulatory mechanism that is exploited by EF-G to promote tRNA movements during translocation, as well as by antibiotics targeting the ribosome that impede this process. Beyond elongation, the initiation, termination, and ribosome recycling stages of protein synthesis all involve transitions between GS1 and GS2 (Agrawal et al., 2004; Klaholz et al., 2004; Allen et al., 2005; Gao et al., 2005; Myasnikov et al., 2005; Gao et al., 2007). Indeed, smFRET experiments using an inter-subunit FRET signal have demonstrated how initiation factors, particularly initiation factor 2, regulate functionally important inter-subunit dynamics during the assembly of an elongation competent ribosomal initiation complex during translation initiation (Marshall et al., 2009). Likewise, smFRET experiments have revealed how release factors and ribosome recycling factor rectify and thereby regulate the thermally activated GS1/GS2 dynamic equilibrium during the termination and ribosome recycling stages of protein synthesis (Sternberg et al., 2009). Therefore, modulation of the ribosome's global architecture through factor-dependent shifts in the translational machinery's conformational equilibria may serve as a general paradigm for translation regulation throughout all stages of protein synthesis.

4. Conclusions and future perspectives

In this chapter we have presented a basic overview of smFRET, including a discussion of the advantages and limitations of applying this biophysical technique to studies of the structural dynamics of protein synthesis. Using the translocation step of translation elongation as an example, we have described how smFRET experiments enable time-resolved observations of large-scale conformational rearrangements of the translational machinery, providing a unique opportunity to thermodynamically and kinetically characterize conformational processes that, while fundamental to the mechanism of protein synthesis, are generally obscured in ensemble studies. Beyond these smFRET studies of translocation, the donor-acceptor pairs described here as well as additional donor-acceptor pairs developed using fluorescence-labeled ribosomes, tRNAs, and translation factors are enabling a rapidly growing number of smFRET investigations of specific conformational processes encompassing every stage of protein synthesis (recently reviewed in (Aitken et al., 2010; Frank and Gonzalez, 2010)).

A major theme emerging from the collective body of smFRET studies of protein synthesis is the stochastic nature of individual steps within the mechanism of translation, in which thermal fluctuations of the ribosome and its tRNA substrates permit sampling of meta-stable conformational states on a complex multi-dimensional free energy landscape (Munro et al., 2009; Fischer et al., 2010; Frank and Gonzalez, 2010). An additional major theme is the ability of translation factors to regulate and direct the conformational equilibria of the ribosomal particle and its tRNA substrates throughout all stages of protein synthesis. By accelerating/decelerating particular conformational transitions and stabilizing/destabilizing particular conformational states, translation factors guide the directionality of conformational processes intrinsic to the ribosome-tRNA complex (Frank and Gonzalez, 2010). In an analogous way, smFRET characterization of the effect of antibiotics on the conformational dynamics of the translational machinery is revealing that these drugs often exert their inhibitory activities through the inhibition of the large-scale structural rearrangements that are required for protein synthesis to proceed rapidly.

Looking to the future, the dynamics of many mechanistically important, highly mobile ribosomal domains remain to be characterized using smFRET. Likewise, many functionally important conformational changes of the translational machinery have been suggested by structural work but have yet to be investigated using smFRET. A particularly exciting example is provided by the L7/L12 protein stalk of the 50S subunit's GTPase-associated center, which is thought to recruit translation factors to the ribosome and control biochemical steps such as GTP hydrolysis and inorganic phosphate release (Mohr et al., 2002; Savelsbergh et al., 2005). Characterizing the nature and timescale of L7/L12 stalk movements with respect to the ribosome, as well as the organization and timing of its interactions with translation factors throughout all stages of protein synthesis would greatly advance our mechanistic understanding of this universally conserved and essential structural element of the ribosome. Similarly, smFRET provides a means with which to characterize the thermodynamics and kinetics underlying putative

movements of the head domain of the 30S subunit, which have been suggested to play important regulatory roles during translation initiation (Carter et al., 2001) as well as during the aa-tRNA selection (Ogle et al., 2002) and translocation (Spahn et al., 2004) steps of translation elongation.

Efforts to obtain a complete mechanistic understanding of the structural dynamics of the translating ribosome will benefit from the development of new technologies and experimental platforms. Recent advances, such as: (i) three-wavelength experiments using multiple donors and acceptors (Hohng et al., 2004) allowing simultaneous tracking of multiple conformational changes and investigation of the degree of conformational coupling within the translational machinery (Munro et al., 2010a; Munro et al., 2010b); (ii) new illumination strategies enabling single-molecule detection of surface-tethered, fluorescence-labeled biomolecules in a physiologically relevant, micromolar background concentration of freely diffusing, fluorescence-labeled ligands (Levene et al., 2003; Uemura et al., 2010); and (iii) new data analysis algorithms permitting increasingly unbiased analysis of smFRET trajectories (Bronson et al., 2009), will allow ever more complex mechanistic questions to be addressed. We envision that these advances will be particularly important in extending smFRET techniques from the studies of prokaryotic protein synthesis described here to studies of the significantly more complex and highly regulated translational machinery of eukaryotic organisms.

Acknowledgements

Work in the Gonzalez laboratory is supported by a Burroughs Wellcome Fund CABS Award (CABS 1 004 856), an NSF CAREER Award (MCB 0 644 262), an NIH-NIGMS grant (GM 084 288 – 01), and an American Cancer Society Research Scholar Grant (RSG GMC-117 152) to R. L. G. We thank Dr. Jingyi Fei, Ms. Margaret Elvekrog, and Prof. Dmitri Ermolenko for critically reading and commenting on the chapter and all members of the Gonzalez laboratory for many incisive discussions.

References

Agirrezabala X, Lei J, Brunelle JL, Ortiz-Meoz RF, Green R, Frank J. (2008) Visualization of the hybrid state of tRNA binding promoted by spontaneous ratcheting of the ribosome. Mol Cell 32: 190–197

Agrawal RK, Sharma MR, Kiel MC, Hirokawa G, Booth TM, Spahn CM, Grassucci RA, Kaji A, Frank J. (2004) Visualization of ribosome-recycling factor on the Escherichia coli 70S ribosome: functional implications. Proc Natl Acad Sci U S A 101: 8900 – 8905

Aitken CE, Marshall RA, Puglisi JD. (2008) An oxygen scavenging system for improvement of dye stability in single-molecule fluorescence experiments. Biophys J 94: 1826–1835

Aitken CE, Petrov A, Puglisi J. (2010) Ribosome dynamics and translation. Annual Review of Biophysics In press

Aitken CE, Puglisi JD. (2010) Following the intersubunit conformation of the ribosome during translation in real time. Nat Struct Mol Biol 17: 793 – 800

Allen GS, Zavialov A, Gursky R, Ehrenberg M, Frank J. (2005) The cryo-EM structure of a translation initiation complex from Escherichia coli. Cell 121: 703–712

Andrec M, Levy RM, Talaga DS. (2003) Direct Determination of Kinetic Rates from Single-Molecule Photon Arrival Trajectories Using Hidden Markov Models. J Phys Chem A 107: 7454–7464

Axelrod D. 2003. Total internal reflection fluorescence microscopy in cell biology. *Biophotonics, Pt B*. San Diego: Academic Press Inc. pp 1–33

Axelrod D, Burghardt TP, Thompson NL. (1984) Total internal-reflection fluorescence. Annual Review of Biophysics and Bioengineering 13: 247–268

Benesch RE, Benesch R. (1953) Enzymatic removal of oxygen for polarography and related methods. Science 118: 447–448

Bergemann K, Nierhaus KH. (1983) Spontaneous, elongation factor G independent translocation of Escherichia coli ribosomes. J Biol Chem 258: 15105–15113

Beringer M, Rodnina MV. (2007) The ribosomal peptidyl transferase. Mol Cell 26: 311–321

Blanchard SC, Gonzalez RL, Kim HD, Chu S, Puglisi JD. (2004a) tRNA selection and kinetic proofreading in translation. Nat Struct Mol Biol 11: 1008–1014

Blanchard SC, Kim HD, Gonzalez RL, Jr., Puglisi JD, Chu S. (2004b) tRNA dynamics on the ribosome during translation. Proc Natl Acad Sci U S A 101: 12 893–12 898

Blanco M, Walter NG. (2010) Analysis of complex single-molecule FRET time trajectories. Methods Enzymol 472: 153–178

Borowski C, Rodnina MV, Wintermeyer W. (1996) Truncated elongation factor G lacking the G domain promotes translocation of the 3' end but not of the anticodon domain of peptidyl-tRNA. Proc Nat Acad Sci USA 93: 4202 – 4206

Bremer H, Dennis PP. 1987. Modulation of chemical composition and other parameters of the cell by growth rate. In: Neidhardt FC, ed. *Escherichia coli and Salmonella typhimurium: cellular and molecular biology*. Washington, DC: American Society for Microbiology. pp 1553–1569

Bretscher MS. (1968) Translocation in protein synthesis: a hybrid structure model. Nature 218: 675 – 677

Bronson JE, Fei J, Hofman JM, Gonzalez Jr. RL, Wiggins CH. (2009) Learning rates and states from biophysical time series: A Bayesian approach to model selection and single-molecule FRET data. Biophys J 97: 3196 – 3205

Carter AP, Clemons WM, Brodersen DE, Morgan-Warren RJ, Wimberly BT, Ramakrishnan V. (2000) Functional insights from the structure of the 30S ribosomal subunit and its interactions with antibiotics. Nature 407: 340 – 348

Carter AP, Clemons WM, Jr., Brodersen DE, Morgan-Warren RJ, Hartsch T, Wimberly BT, Ramakrishnan V. (2001) Crystal structure of an initiation factor bound to the 30S ribosomal subunit. Science 291: 498 – 501

Clamme JP, Deniz AA. (2005) Three-color single-molecule fluorescence resonance energy transfer. Chemphyschem 6: 74–77

Clegg RM. (1995) Fluorescence resonance energy transfer. Curr Opin Biotechnol 6: 103–110

Colquhoun D, Hawkes AG. 1995. The principles of the stochastic interpretation of ion-channel mechanism. In: Sakmann B, Heher E, eds. *Single Channel Recording*. New York: Plenum Press. pp 397–482

Cornish PV, Ermolenko DN, Noller HF, Ha T. (2008) Spontaneous intersubunit rotation in single ribosomes. Mol Cell 30: 578–588

Cornish PV, Ermolenko DN, Staple DW, Hoang L, Hickerson RP, Noller HF, Ha T. (2009) Following movement of the L1 stalk between three functional states in single ribosomes. Proc Natl Acad Sci U S A 106: 2571–2576

Cornish PV, Ha T. (2007) A survey of single-molecule techniques in chemical biology. ACS Chem Biol 2: 53–61

Dave R, Terry DS, Munro JB, Blanchard SC. (2009) Mitigating unwanted photophysical processes for improved single-molecule fluorescence imaging. Biophys J 96: 2371–2381

Dorner S, Brunelle JL, Sharma D, Green R. (2006) The hybrid state of tRNA binding is an authentic translation elongation intermediate. Nat Struct Mol Biol 13: 234–241

Dorywalska M, Blanchard SC, Gonzalez Jr. RL, Kim HD, Chu S, Puglisi JD. (2005) Site-specific labeling of the ribosome for single-molecule spectroscopy. Nucleic Acids Res 33: 182–189

Draper DE. (2004) A guide to ions and RNA structure. Rna 10: 335–343

Dunkle JA, Cate JH. (2010) Ribosome structure and dynamics during translocation and termination. Annu Rev Biophys 39: 227–244

Ermolenko DN, Majumdar ZK, Hickerson RP, Spiegel PC, Clegg RM, Noller HF. (2007a) Observation of intersubunit movement of the ribosome in solution using FRET. J Mol Biol 370: 530–540

Ermolenko DN, Spiegel PC, Majumdar ZK, Hickerson RP, Clegg RM, Noller HF. (2007b) The antibiotic viomycin traps the ribosome in an intermediate state of translocation. Nat Struct Mol Biol 14: 493–497

Fei J, Bronson JE, Hofman JM, Srinivas RL, Wiggins CH, Gonzalez RLJ. (2009) Allosteric collaboration between elongation factor G and the ribosomal L1 stalk directs tRNA movements during translation. Proc Natl Acad Sci U S A 106: 15702–15707

Fei J, Kosuri P, MacDougall DD, Gonzalez RL, Jr. (2008) Coupling of ribosomal L1 stalk and tRNA dynamics during translation elongation. Mol Cell 30: 348–359

Fei J, Wang J, Sternberg SH, MacDougall DD, Elvekrog MM, Pulukkunat DK, Englander MT, Gonzalez RL, Jr. (2010) A highly purified, fluorescently labeled in vitro translation system for single-molecule studies of protein synthesis. Methods Enzymol 472: 221–259

Feldman MB, Terry DS, Altman RB, Blanchard SC. (2010) Aminoglycoside activity observed on single pre-translocation ribosome complexes. Nat Chem Biol 6: 54–62

Fischer N, Konevega AL, Wintermeyer W, Rodnina MV, Stark H. (2010) Ribosome dynamics and tRNA movement by time-resolved electron cryomicroscopy. Nature 466: 329–333

Förster T. (1946) Energiewanderung und fluoreszenz. Naturwissenschaften 33: 166–175

Frank J, Agrawal RK. (2000) A ratchet-like inter-subunit reorganization of the ribosome during translocation. Nature 406: 318–322

Frank J, Gao H, Sengupta J, Gao N, Taylor DJ. (2007) The process of mRNA-tRNA translocation. Proc Natl Acad Sci U S A 104: 19 671–19 678

Frank J, Gonzalez RL, Jr. (2010) Structure and dynamics of a processive Brownian motor: the translating ribosome. Annu Rev Biochem 79: 381–412

Gao H, Zhou Z, Rawat U, Huang C, Bouakaz L, Wang C, Cheng Z, Liu Y, Zavialov A, Gursky R, Sanyal S, Ehrenberg M, Frank J, Song H. (2007) RF3 induces ribosomal conformational changes responsible for dissociation of class I release factors. Cell 129: 929–941

Gao N, Zavialov AV, Li W, Sengupta J, Valle M, Gursky RP, Ehrenberg M, Frank J. (2005) Mechanism for the disassembly of the posttermination complex inferred from cryo-EM studies. Mol Cell 18: 663–674

Gavrilova LP, Kostiashkina OE, Koteliansky VE, Rutkevitch NM, Spirin AS. (1976) Factor-free ("non-enzymic") and factor-dependent systems of translation of polyuridylic acid by Escherichia coli ribosomes. J Mol Biol 101: 537–552

Gavrilova LP, Spirin AS. (1971) Stimulation of "non-enzymic" translocation in ribosomes by p-chloromercuribenzoate. FEBS Lett 17: 324–326

Gonzalez Jr. RL, Chu S, Puglisi JD. (2007) Thiostrepton inhibition of tRNA delivery to the ribosome. RNA 13: 2091–2097

Gromadski KB, Rodnina MV. (2004) Kinetic determinants of high-fidelity tRNA discrimination on the ribosome. Mol Cell 13: 191–200

Ha T. (2001) Single-Molecule Fluorescence Resonance Energy Transfer. Methods 25: 78–86

Ha T, Rasnik I, Cheng W, Babcock HP, Gauss GH, Lohman TM, Chu S. (2002) Initiation and re-initiation of DNA unwinding by the Escherichia coli Rep helicase. Nature 419: 638–641

Hohng S, Joo C, Ha T. (2004) Single-molecule three-color FRET. Biophys J 87: 1328–1337

Horan LH, Noller HF. (2007) Intersubunit movement is required for ribosomal translocation. Proc Natl Acad Sci U S A 104: 4881–4885

Hubner CG, Renn A, Renge I, Wild UP. (2001) Direct observation of the triplet lifetime quenching of single dye molecules by molecular oxygen. Journal of Chemical Physics 115: 9619–9622

Hwang LC, Hohlbein J, Holden SJ, Kapanidis AN. 2009. Single-molecule FRET: Methods and biological applications. In: Hinterdorfer P, van Oijen AM, eds. *Handbook of Single-Molecule Biophysics*. New York: Springer. pp 130–132

Jares-Erijman EA, Jovin TM. (2003) FRET imaging. Nat Biotechnol 21: 1387–1395

Johansen SK, Maus CE, Plikaytis BB, Douthwaite S. (2006) Capreomycin binds across the ribosomal subunit interface using tlyA-encoded 2'-O-methylations in 16S and 23S rRNAs. Mol Cell 23: 173–182

Johnson AE, Adkins HJ, Matthews EA, Cantor CR. (1982) Distance moved by transfer RNA during translocation from the A site to the P site on the ribosome. J Mol Biol 156: 113–140

Joo C, Ha T. 2007. Single-molecule FRET with total internal reflection microscopy. In: Selvin PR, Ha T, eds. *Single Molecule Techniques: a Laboratory Manual*. Cold Spring Harbor, New York: Cold Spring Harbor Laboratory Press. pp 3–36

Julian P, Konevega AL, Scheres SH, Lazaro M, Gil D, Wintermeyer W, Rodnina MV, Valle M. (2008) Structure of ratcheted ribosomes with tRNAs in hybrid states. Proc Natl Acad Sci U S A 105: 16924–16927

Katunin VI, Savelsbergh A, Rodnina MV, Wintermeyer W. (2002) Coupling of GTP hydrolysis by elongation factor G to translocation and factor recycling on the ribosome. Biochemistry 41: 12806–12812

Kennell D, Riezman H. (1977) Transcription and translation initiation frequencies of the Escherichia coli lac operon. J Mol Biol 114: 1–21

Kim HD, Puglisi J, Chu S. (2007) Fluctuations of transfer RNAs between classical and hybrid states. Biophys J 93: 3575–3582

Klaholz BP, Myasnikov AG, Van Heel M. (2004) Visualization of release factor 3 on the ribosome during termination of protein synthesis. Nature 427: 862–865

Konevega AL, Fischer N, Semenkov YP, Stark H, Wintermeyer W, Rodnina MV. (2007) Spontaneous reverse movement of mRNA-bound tRNA through the ribosome. Nat Struct Mol Biol 14: 318–324

Korostelev A, Ermolenko DN, Noller HF. (2008) Structural dynamics of the ribosome. Curr Opin Chem Biol

Levene MJ, Korlach J, Turner SW, Foquet M, Craighead HG, Webb WW. (2003) Zero-mode waveguides for single-molecule analysis at high concentrations. Science 299: 682–686

Liang ST, Xu YC, Dennis P, Bremer H. (2000) mRNA composition and control of bacterial gene expression. J Bacteriol 182: 3037–3044

Liu Y, Park J, Dahmen KA, Chemla YR, Ha T. (2010) A comparative study of multivariate and univariate hidden Markov modelings in time-binned single-molecule FRET data analysis. J Phys Chem B 114: 5386–5403

Marshall RA, Aitken CE, Puglisi JD. (2009) GTP hydrolysis by IF2 guides progression of the ribosome into elongation. Mol Cell 35: 37–47

Marshall RA, Dorywalska M, Puglisi JD. (2008) Irreversible chemical steps control intersubunit dynamics during translation. Proc Natl Acad Sci U S A 105: 15364–15369

McKinney SA, Joo C, Ha T. (2006) Analysis of single-molecule FRET trajectories using hidden Markov modeling. Biophys J 91: 1941–1951

Moazed D, Noller HF. (1987) Chloramphenicol, erythromycin, carbomycin and vernamycin B protect overlapping sites in the peptidyl transferase region of 23S ribosomal RNA. Biochimie 69: 879–884

Moazed D, Noller HF. (1989) Intermediate states in the movement of transfer RNA in the ribosome. Nature 342: 142–148

Mohr D, Wintermeyer W, Rodnina MV. (2002) GTPase activation of elongation factors Tu and G on the ribosome. Biochemistry 41: 12 520–12 528

Moran-Mirabal JM, Craighead HG. (2008) Zero-mode waveguides: sub-wavelength nanostructures for single molecule studies at high concentrations. Methods 46: 11–17

Munro JB, Altman RB, O'Connor N, Blanchard SC. (2007) Identification of two distinct hybrid state intermediates on the ribosome. Mol Cell 25: 505–517

Munro JB, Altman RB, Tung CS, Cate JH, Sanbonmatsu KY, Blanchard SC. (2010a) Spontaneous formation of the unlocked state of the ribosome is a multistep process. Proc Natl Acad Sci U S A 107: 709–714

Munro JB, Altman RB, Tung CS, Sanbonmatsu KY, Blanchard SC. (2010b) A fast dynamic mode of the EF-G-bound ribosome. Embo J In press

Munro JB, Sanbonmatsu KY, Spahn CM, Blanchard SC. (2009) Navigating the ribosome's metastable energy landscape. Trends Biochem Sci 34: 390–400

Myasnikov AG, Marzi S, Simonetti A, Giuliodori AM, Gualerzi CO, Yusupova G, Yusupov M, Klaholz BP. (2005) Conformational transition of initiation factor 2from the GTP- to GDP-bound state visualized on the ribosome. Nat Struct Mol Biol 12: 1145–1149

Odom OW, Picking WD, Hardesty B. (1990) Movement of tRNA but not the nascent peptide during peptide bond formation on ribosomes. Biochemistry 29: 10734–10744

Ogle JM, Murphy FV, Tarry MJ, Ramakrishnan V. (2002) Selection of tRNA by the ribosome requires a transition from an open to a closed form. Cell 111: 721–732

Pan D, Kirillov S, Zhang CM, Hou YM, Cooperman BS. (2006) Rapid ribosomal translocation depends on the conserved 18–55 base pair in P-site transfer RNA. Nat Struct Mol Biol 13: 354–359

Pan D, Kirillov SV, Cooperman BS. (2007) Kinetically competent intermediates in the translocation step of protein synthesis. Mol Cell 25: 519–529

Pape T, Wintermeyer W, Rodnina MV. (1998) Complete kinetic mechanism of elongation factor Tu-dependent binding of aminoacyl-tRNA to the A site of the *E. coli* ribosome. EMBO (Eur Mol Biol Organ) J 17: 7490–7497

Patil PV, Ballou DP. (2000) The use of protocatechuate dioxygenase for maintaining anaerobic conditions in biochemical experiments. Anal Biochem 286: 187–192

Paulsen H, Robertson JM, Wintermeyer W. (1983) Topological arrangement of two transfer RNAs on the ribosome: fluorescence energy transfer measurements between A and P site-bound $tRNA^{Phe}$. J Mol Biol 167: 411–426

Pawley JB. 2006. *Handbook of Biological Confocal Microscopy*. New York City: Springer

Peske F, Savelsbergh A, Katunin VI, Rodnina MV, Wintermeyer W. (2004) Conformational changes of the small ribosomal subunit during elongation factor G-dependent tRNA-mRNA translocation. J Mol Biol 343: 1183–1194

Pestka S. (1969) Studies on the formation of transfer ribonucleic acid-ribosome complexes. VI. Oligopeptide synthesis and translocation on ribosomes in the presence and absence of soluble transfer factors. J Biol Chem 244: 1533–1539

Piwonski H, Kolos R, Meixner A, Sepiol J. (2005) Optimal oxygen concentration for the detection of single indocarbocyanine molecules in a polymeric matrix. Chemical Physics Letters 405: 352–356

Proshkin S, Rahmouni AR, Mironov A, Nudler E. (2010) Cooperation between translating ribosomes and RNA polymerase in transcription elongation. Science 328: 504–508

Qin F, Auerbach A, Sachs F. (1996) Estimating single-channel kinetic parameters from idealized patch-clamp data containing missed events. Biophys J 70: 264–280

Rasnik I, McKinney SA, Ha T. (2005) Surfaces and orientations: much to FRET about? Acc Chem Res 38: 542–548

Renn A, Seelig J, Sandoghdar V. (2006) Oxygen-dependent photochemistry of fluorescent dyes studied at the single molecule level. Molecular Physics: An International Journal at the Interface Between Chemistry and Physics 104: 409–414

Rodnina MV, Gromadski KB, Kothe U, Wieden HJ. (2005) Recognition and selection of tRNA in translation. FEBS Lett 579: 938–942

Rodnina MV, Savelsbergh A, Katunin VI, Wintermeyer W. (1997) Hydrolysis of GTP by elongation factor G drives tRNA movement on the ribosome. Nature 385: 37–41

Roy R, Hohng S, Ha T. (2008) A practical guide to single-molecule FRET. Nat Methods 5: 507–516

Savelsbergh A, Katunin VI, Mohr D, Peske F, Rodnina MV, Wintermeyer W. (2003) An elongation factor G-induced ribosome rearrangement precedes tRNA-mRNA translocation. Mol Cell 11: 1517–1523

Savelsbergh A, Mohr D, Kothe U, Wintermeyer W, Rodnina MV. (2005) Control of phosphate release from elongation factor G by ribosomal protein L7/12. Embo J 24: 4316–4323

Selvin PR. (1995) Fluorescence resonance energy transfer. Methods Enzymol 246: 300–334

Selvin PR. (2000) The renaissance of fluorescence resonance energy transfer. Nat Struct Biol 7: 730–734

Shoji S, Walker SE, Fredrick K. (2006) Reverse translocation of tRNA in the ribosome. Mol Cell 24: 931–942

Shoji S, Walker SE, Fredrick K. (2009) Ribosomal Translocation: One Step Closer to the Molecular Mechanism. ACS Chem Biol 27: 27

Sorensen MA, Pedersen S. (1991) Absolute in vivo translation rates of individual codons in Escherichia coli. The two glutamic acid codons GAA and GAG are translated with a threefold difference in rate. J Mol Biol 222: 265–280

Spahn CM, Gomez-Lorenzo MG, Grassucci RA, Jorgensen R, Andersen GR, Beckmann R, Penczek PA, Ballesta JP, Frank J. (2004) Domain movements of elongation factor eEF2 and the eukaryotic 80S ribosome facilitate tRNA translocation. Embo J 23: 1008–1019

Spirin AS. (1968) How does the ribosome work? A hypothesis based on the two subunit construction of the ribosome. Curr Mod Biol 2: 115–127

Spirin AS. (1985) Ribosomal translocation: facts and models. Progress in Nucleic Acid Research & Molecular Biology 32: 75–114

Spirin AS. (2002) Ribosome as a molecular machine. FEBS Lett 514: 2–10

Stanley RE, Blaha G, Grodzicki RL, Strickler MD, Steitz TA. (2010) The structures of the anti-tuberculosis antibiotics viomycin and capreomycin bound to the 70S ribosome. Nat Struct Mol Biol 17: 289–293

Sternberg SH, Fei J, Prywes N, McGrath KA, Gonzalez RL, Jr. (2009) Translation factors direct intrinsic ribosome dynamics during translation termination and ribosome recycling. Nat Struct Mol Biol 16: 861–868

Subramanian AR, Dabbs ER. (1980) Functional studies on ribosomes lacking protein L-1from mutant escherichia coli. Eur J Biochem 112: 425–430

Talaga DS. (2007) COCIS: Markov processes in single molecule fluorescence. Curr Opin Colloid Interface Sci 12: 285–296

Traut RR, Monro RE. (1964) The Puromycin Reaction and its Relation to Protein Synthesis. J Mol Biol 10: 63–72

Uemura S, Aitken CE, Korlach J, Flusberg BA, Turner SW, Puglisi JD. (2010) Real-time tRNA transit on single translating ribosomes at codon resolution. Nature 464: 1012–1017

Uemura S, Dorywalska M, Lee TH, Kim HD, Puglisi JD, Chu S. (2007) Peptide bond formation destabilizes Shine-Dalgarno interaction on the ribosome. Nature 446: 454–457

Valle M, Zavialov AV, Sengupta J, Rawat U, Ehrenberg M, Frank J. (2003) Locking and unlocking of ribosomal motions. Cell 114: 123–134

Wang Y, Qin H, Kudaravalli RD, Kirillov SV, Dempsey GT, Pan D, Cooperman BS, Goldman YE. (2007) Single-molecule structural dynamics of EF-G–ribosome interaction during translocation. Biochemistry 46: 10 767–10 775

Wu P, Brand L. (1994) Resonance energy transfer: methods and applications. Anal Biochem 218: 1–13

Yamada T, Mizugichi Y, Nierhaus KH, Wittmann HG. (1978) Resistance to viomycin conferred by RNA of either ribosomal subunit. Nature 275: 460–461

Zhang W, Dunkle JA, Cate JH. (2009) Structures of the ribosome in intermediate states of ratcheting. Science 325:1014–1017